J Biol Inorg Chem (2016) 21:241–249
DOI 10.1007/s00775-015-1331-x

ORIGINAL PAPER

Iron overload of human colon adenocarcinoma cells studied by synchrotron-based X-ray techniques

Victor G. Mihucz[1] · Florian Meirer[2] · Zsófia Polgári[1] · Andrea Réti[3] · Giancarlo Pepponi[4] · Dieter Ingerle[5] · Norbert Szoboszlai[1] · Christina Streli[5]

Received: 22 May 2015 / Accepted: 30 December 2015 / Published online: 13 January 2016

Abstract Fast- and slow-proliferating human adenocarcinoma colorectal cells, HT-29 and HCA-7, respectively, overloaded with transferrin (Tf), Fe(III) citrate, Fe(III) chloride and Fe(II) sulfate were studied by synchrotron radiation total-reflection X-ray spectrometry (TXRF), TXRF-X-ray absorption near edge structure (TXRF-XANES), and micro-X-ray fluorescence imaging to obtain information on the intracellular storage of overloaded iron (Fe). The determined TfR1 mRNA expression for the investigated cells correlated with their proliferation rate. In all cases, the Fe XANES of cells overloaded with inorganic Fe was found to be similar to that of deliquescent Fe(III) sulfate characterized by a distorted octahedral geometry. A fitting model using a linear combination of the XANES of Tf and deliquescent Fe(III) sulfate allowed to explain the near edge structure recorded for HT-29 cells indicating that cellular overload with inorganic Fe results in a non-ferritin-like fast Fe storage. Hierarchical cluster analysis of XANES spectra recorded for Fe overloaded HT-29 and HCA-7 cells was able to distinguish between Fe treatments performed with different Fe species with a 95 % hit rate, indicating clear differences in the Fe storage system. Micro-X-ray fluorescence imaging of Fe overloaded HT-29 cells revealed that Fe is primarily located in the cytosol of the cells. By characterizing the cellular Fe uptake, Fe/S content ratios were calculated based on the X-ray fluorescence signals of the analytes. These Fe/S ratios were dramatically lower for HCA-7 treated with organic Fe(III) treatments suggesting dissimilarities from the Tf-like Fe uptake.

Keywords Cancer cells · Fe storage · Micro-X-ray imaging · Transferrin

Introduction

Iron (Fe) is involved in several primary cellular functions such as DNA synthesis, ATP generation, electron transfer, and oxidation of substrates. Because Fe is essential for cell survival and replication [1] and both Fe overload and deficiency can cause cellular death, homeostatic mechanisms tightly control its intestinal absorption, systemic transport, cellular uptake, storage and cellular efflux [2]. Most cellular Fe is firmly bound to components such as hemoglobin, heme, ferritin, transferrin (Tf) and various enzymes. Among these compounds, Tf is the major Fe-binding protein in the blood plasma. The main pathway for Fe uptake by animal cells is through Tf and its specific receptor (TfR), located at the cell surface. Iron release involves endosomal acidification through an ATP-dependent proton pump and reduction

Electronic supplementary material The online version of this article (doi:10.1007/s00775-015-1331-x) contains supplementary material, which is available to authorized users.

✉ Norbert Szoboszlai
szobosz@chem.elte.hu

[1] Laboratory of Environmental Chemistry and Bioanalytics, Department of Analytical Chemistry, Institute of Chemistry, Eötvös Loránd University, Pázmány Péter stny 1/A, 1117 Budapest, Hungary

[2] Inorganic Chemistry and Catalysis, Debye Institute for Nanomaterials Science, Utrecht University, Universiteitsweg 99, 3584 CG Utrecht, The Netherlands

[3] 2nd Department of Pathology, Semmelweis University, Üllői út 93, 1091 Budapest, Hungary

[4] Micro Nano Analytical Laboratory, Centre for Materials and Microsystems, Fondazione Bruno Kessler, Povo, Via Sommarive 18, 38123 Trento, Italy

[5] Atominstitut, Technische Universitaet Wien, Stadionallee 2, 1020 Vienna, Austria

of Fe(III) ions to the more soluble Fe(II) form by endosomal ferrireductase-like STEAP family members [3–6]. Besides Tf-bound Fe, animal cells can also obtain Fe from small, low molecular weight complexes. The composition and quantity of these low affinity ligands may vary under different physiological conditions. This non-Tf-bound Fe, also called labile Fe pool, is generated under conditions of Fe overload, when the binding capacity of Tf is saturated [7–9]. The labile Fe pool is localized primarily in the cytosol. Cells maintain organellar pools of labile Fe despite its propensity for catalyzing reactive oxygen species formation. Among transmembrane Fe transporters, divalent metal transporter 1 (DMT1) and Zip14 were reported to be involved in the non-Tf-bound Fe uptake [10, 11]. Iron(II) ions are transported into cells by DMT1 optimally at pH 5.5. Moreover, DMT1 also mediates the recovery of Fe from acidified endosomes during the Tf-TfR recycling process [11, 12]. Thus, replenishment of cytosolic labile Fe in mammalian cells includes: (1) export from the endosome by the DMT1; (2) reductive release of Fe from Fe(III)-Tf; (3) degradation of the long-term Fe storage protein ferritin; (4) release from heme and heme proteins [13].

Due to its inherently transient nature and susceptibility to undergo ligand exchange reactions and redox conversions, quantification or even characterization of labile Fe is difficult. Radiolabeled Fe can be traced inside the cell following cell fractionation [9, 14]. The use of fluorescein and rhodamine derivatives as fluorophores loaded into living cells that bind to the complexes of labile Fe and subsequent stoichiometric fluorescence quenching is another technique suitable for Fe determination [9, 13, 15–18]. In fact, the quantity of the chelatable Fe pool is defined by the stability constant of the complex formed by the chelator used for its detection [16, 18], and by applying fluorescence, only the labile Fe pool can be determined, but no information on its chemical structure can be obtained, since the fluorescent chelator causes the quenching of Fe from the biological bond. Moreover, the aforementioned fluorescent technique supplies only indirect information on the localization of cytosolic labile Fe, since the Fe and protein bond are quenched due to the inherent nature of this technique.

Total-reflection X-ray fluorescence spectrometry (TXRF) proved to be suitable for intracellular Fe determination in colorectal cells [19, 20]. Information on elemental speciation can be provided by combining it with X-ray absorption near edge structure (XANES) spectroscopy, which requires the use of a synchrotron radiation (SR) source. X-ray fluorescence acquisition in total-reflection geometry can be exploited for the acquisition of X-ray absorption spectra of trace elements in minute samples, for instance, containing typically 10 ng Fe [21]. The energy of incident X-rays is tuned around the absorption edge energy of the studied element (i.e., 7112 eV for the Fe K-edge). Thus, the TXRF-XANES has proved to be suitable for investigation of Fe containing proteins such as ferritin [22]. Ensuring an in situ speciation, TXRF-XANES does not require tedious sample preparation prone to modify the chemical element species (e.g., cell fractionation). However, stability of element species from sample preparation to storage and analysis should be tested systematically with standards of known oxidation state for the element of interest. The X-ray focusing optics can be used with submicrometric beams of high photon densities and allow X-ray fluorescence imaging.

The objective of this study was to obtain reliable information on the distribution, temporary storage and localization of intracellular Fe within cancer cells under in vitro simulated Fe overload conditions. To achieve this, two different human colorectal adenocarcinoma cells, HT-29 and HCA-7, were used due to their different proliferation rate treating them with inorganic and organic Fe(II/III) compounds in a concentration of 50 μmol Fe/L for 4 and 24 h. Comparison of XANES spectra of Fe overloaded cancer cells was used to obtain information on the temporary Fe storage.

Materials and methods

Cell cultures and sample preparation

Human colon adenocarcinoma cell lines—HT-29 and HCA-7—were grown at the 2nd Institute of Pathology, Budapest, Hungary in 37 °C in a humidified atmosphere consisting of 5 % v/v CO_2 in an antibiotic-free medium supplemented with 10 % v/v fetal calf serum (FCS) supplied by Sigma-Aldrich (St. Louis, MO, USA). The HT-29 and HCA-7 cells were obtained from ECACC (European Collection of Cell Cultures, UK). For the growth of HT-29 and HCA-7 cells, RPMI-1640 (Roswell Park Memorial Institute) and DMEM (Dulbecco's Modified Eagle Medium) growth media were used, respectively.

The reagent grade Tf, Fe(III) citrate, ethylene diamine tetraacetic acid (EDTA), Fe(III) chloride, Fe(II) sulfate and Fe(III) sulfate hydrate standards were supplied by Sigma-Aldrich. For the TXRF-XANES experiments, on one hand, Fe(III) sulfate hydrate was used in the solid state of matter referred further in the manuscript as deliquescent Fe(III) sulfate. On the other hand, this deliquescent Fe(III) sulfate was dissolved either in deionized water or dimethyl sulfoxide (DMSO), referred further as Fe(III) sulfate (aq) and Fe(III) sulfate (DMSO), respectively. The concentration of the latter two Fe(III) sulfate stock solutions was 10 mg/L for Fe. From each stock solution, 1 μL containing 10 ng of Fe was pipetted directly onto the quartz reflectors and dried immediately.

Cells were cultured to 80 % confluency, then incubated for 4 or 24 h with 50 μmol/L (expressed as Fe in medium) Fe(II) sulfate, Fe(III) chloride, Fe(III) citrate and Tf, harvested by trypsin, washed twice with an isotonic NaCl solution and, finally, centrifuged at 20,000*g* and 4 °C for 15 min. Then, the cells were resuspended in 10 μL of isotonic NaCl solution. Five μL of cell suspension was pipetted onto quartz plates. The estimated cell concentration using a haemocytometer (MOM, Hungary) was 10,000–20,000 cells/μL. The excess of the isotonic NaCl solution was removed by pipetting. After this procedure, the cell monolayer was controlled microscopically. All quartz carrier plates were transported in Ar-filled vessels to the Synchrotronstrahlungslabor HASYLAB SR facility at DESY (Hamburg, Germany).

For X-ray imaging, cells were grown on 7.5 mm × 7.5 mm low stress silicon nitride windows with a thickness of 500 nm supplied by Norcada (Edmonton, AB, Canada). Iron treatments were performed with 50 μM Fe(II) sulfate for 2 h. Then, samples were deep frozen in liquid nitrogen, freeze-dried, and transported to the Diamond Light Source facilities.

Total RNA extraction and cDNA synthesis for real-time RT-PCR

Total RNA was isolated from subconfluent cultures of HT-29 and HCA-7 cells. Total RNA was isolated using Trifast (Peqlab, Erlangen, Germany) according to the protocol of manufacturer. The amount of RNA was determined spectrophotometrically at 260/280 nm by Nano Drop spectrophotometer (Peqlab). The cDNA was synthesized using RevertAid MMuLV reverse transcriptase (Fermentas, Thermo Fisher Scientific, Waltham, MA, USA) and random hexamer primers (GE Healthcare, Pittsburgh, PA, USA).

Quantitative real-time RT-PCR

The TfR mRNA expression was determined by real-time RT-PCR. For the quantification of PCR products, the threshold cycle (CT) was used. The delta CT value was calculated from the difference in the CT of the gene of interest and that of the glyceraldehyde 3-phosphate dehydrogenase (GAPDH) housekeeping gene used as reference. The TfR primers were: (1) forward: 5′-GGCTTTGTAGAACCAGATCA-3′ and (2) reverse: 5′-GGGCAAGTTTCAATAGGAGA-3′ and those for GAPDH were: (1) forward 5′-GTCTCCTCT GACTTCAACAG-3′ and (2) reverse: 5′-CGTTAGC CAAATTCGTTGTC-3′. The amplifications were performed in a mixture of 1 μL of cDNA, 0.3 μL/primers, 2 μL 5 × Hot FirePol Eva Green qPCR Mix Plus (Solis Biodyne, Tartu, Estonia) and 6.4 μL H_2O on a 96-well plate for real-time arrays. Gene expression quantification was performed by ABI PRISM 7500 instrument (Applied Biosystems Carlsbad, CA, USA) using the corresponding software. The 15 min activation of the DNA polymerase at 95 °C was followed by 40 cycles of 25 s denaturation at 95 °C, 30 s annealing at 55 °C and 30 s extension at 72 °C. The amplicon purity was checked by melting curve analysis. Measurements were made in triplicates of two independent experiments. Statistical data analysis was performed by Student's *t* test at the 99 % confidence level, using Origin 7.5 software.

TXRF-XANES

The Fe K-edge XANES measurements in fluorescence mode were carried out in vacuum using the setup at the beamline L at HASYLAB at DESY [23]. A Si(111) double crystal monochromator was used for selecting the energy of the exciting beam from the continuous X-ray spectrum emitted by a 1.2 Tesla bending magnet at beamline L. The primary beam was collimated to 100 μm × 2300 μm (horizontal × vertical) by a cross-slit system. The incident X-ray intensity was monitored with an ionization chamber. For the reproducibility and accuracy of the measurements during all XANES scans, the absorption of an Fe foil was recorded in transmission mode simultaneously. During the analysis, the excitation energy was tuned in varying steps (15, 10, 5 and 1 eV in the pre- and post-edge regions and 0.5 eV across the edge) around the Fe K-edge at 7112 eV. At each energy, a fluorescence spectrum was recorded by a Silicon Drift Detector (SDD, VORTEX 50 mm^2, Radiant Detector Technologies, Northridge, CA, USA) [22–24]. A major challenge in elemental speciation is to avoid chemical transformation during analyses. Therefore, the samples were transported in argon environment. In total, 24 samples treated with different Fe compounds were analyzed by TXRF-XANES. All 30 individual X-ray absorption spectra (24 samples plus 6 references) have been pre-processed and analyzed with the ATHENA software, included in the IFEFFIT program package for XAS analysis [25].

For the characterization of the Fe content of cells, the Fe and S fluorescent signals of the cells were recorded by irradiating the samples with a beam of 10 keV energy for 100 s in TXRF mode. Then, the common logarithm (base 10 logarithm) of the Fe/S ratios was calculated. Quantitative determination of Fe in the cells was not possible using the internal standard calibration method, since intact cells were analyzed. Pipetting aliquots of an adequate internal standard (e.g., gallium or yttrium) solution onto the cells would not have ensured its internal compartmentalization. Thus, the signal of cellular Fe and that of the not compartmentalized internal standard would have resulted in different fluorescent yields. Since the sulfur (S) content of cells correlates with the total protein content and subsequently with the cell number, the S fluorescence of the cells was used as an internal reference element. Since Fe(II) sulfate

is taken up by cells at the μM concentration level and the S content of cells is more than two orders of magnitude higher, contamination from S could be excluded.

Principal component analysis (PCA)–hierarchical clustering

Principal component analysis and hierarchical clustering of the whole series of collected XANES were performed using self-developed code written in the Matlab™ computing language. This multivariate analysis was carried out to pool samples with similar XANES. Data matrix eigendecomposition was achieved by singular value decomposition, and the first six eigenvectors (principal components) explained 99.982 % of the data's variance (cumulative variance explained). Therefore, these six principal components were used as a new basis set spanning the 6-dimensional space in which hierarchical clustering was carried out. Supervised hierarchical agglomerative cluster analysis was performed using Euclidean distances between data points, the unweighted average distance for computing the distance between clusters, and a manually fixed linkage threshold of 0.36 (i.e., 36 % of the maximum linkage distance), effectively pooling individual spectra into clusters containing most similar XANES. Detailed information on PCA–hierarchical clustering can be seen in the electronic supplementary material.

Micro-XRF imaging

Scanning X-ray fluorescence (XRF) microscopy was performed at beamline B16 of the Diamond Light Source (Harwell Science and Innovation Campus, Oxfordshire, UK) according to a previously developed method [26]. White beam excitation with Al filter was chosen to excite elements from Cl to Zn. A Kirkpatrick-Baez focusing optic was used to obtain an X-ray beam with a spot size of 0.5 μm × 1 μm. However, to localize the cells on the membranes, first, a low resolution scan with a beam size of 5 μm × 5 μm of the sample was performed. The XRF spectra from the specimen were acquired with a four-element energy dispersive SDD detector. Spectral analysis of the fluorescence spectrum of each pixel then provided images of the spatial distribution of each element.

Results and discussion

Selection of colorectal cell lines for studying Fe overload

Two colorectal adenocarcinoma cells, namely HT-29 and HCA-7, were selected for the present study. The proliferation rate of HT-29 and HCA-7 cells expressed as the doubling time was approximately 20 h and 36 h, respectively. To date, several studies have found correlation between the rate of cell proliferation and the expression of TfR1 [27, 28]. Since different proliferation rates were observed for HT-29 and HCA-7 cells, their TfR1 mRNA expression was determined by quantitative real-time PCR. As shown in Fig. 1, the TfR1 mRNA expression was significantly higher ($p < 0.01$) in the case of the fast-proliferating HT-29 cells compared to the slow-proliferating HCA-7 ones.

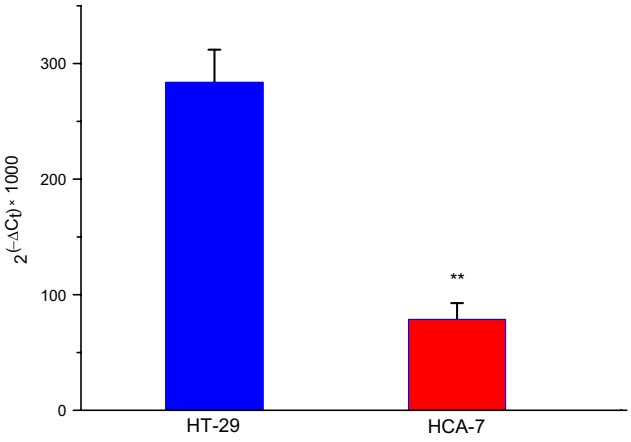

Fig. 1 Transferrin receptor 1 (TfR1) expression of HT-29 and HCA-7 human adenocarcinoma cell lines. Data are presented as $2^{\wedge(-\text{deltaCt})}$ relative to GAPDH; **, HT-29 versus HCA-7, $p < 0.01$

Fe/S ratios in Fe overloaded colorectal adenocarcinoma cells

In our previous studies, we proved that the Fe content of cancer cells grown in FCS or FCS-free culture media varied between 10 and 30 ng/10^6 cells [19, 29]. Unlike Cu and Zn, cells can take up Fe in higher amounts, for example 1500 ng Fe/10^6 cells for HT-29 adenocarcinoma [19]. This phenomenon is known in the literature as Fe overload and it is mostly related to pathological conditions such as haemochromatosis or thalassemia [7, 30, 31]. Relatively large amounts of Fe can be rapidly released, this diffusible labile Fe pool being regarded as the crossroads of cellular Fe traffic [9, 17].

The Fe/S ratios obtained for HT-29 and HCA-7 cells, taken to indirectly characterize cellular Fe uptake, are shown in Fig. 2. The decreasing order in Fe/S ratios according to the different treatments was the same for both cells: Fe(II) sulfate > Fe(III) chloride > Fe(III) citrate > Tf. This is in good agreement with our previous work, where the uptake of Tf and non-Tf type of Fe (Fe(II) sulfate, Fe(III) chloride and Fe(III) citrate) by HT-29 cells in the concentration range of 10–100 μM was studied [19]. Iron uptake from either Fe(II) or Fe(III) inorganic salts was much higher (approximately 25-fold) than from organic Fe compounds [19]. For the Fe(II) sulfate treatment, the Fe/S

ratios were similarly high in the case of both cells. This is understandable, since inorganic Fe(II) is readily absorbed through DMT1 [10]. However, there is a maximum Fe level at the Fe(II) sulfate treatment, and a steady-state equilibrium between uptake and release is achieved. The maximal Fe/S ratio is similar for both cells. Nevertheless, the Fe/S ratio showed considerably big differences at the other treatments. For the HT-29 cell, the $\log_{10}$ Fe/S values were higher than zero for all treatments. The Fe(III) chloride, Fe(III) citrate and Tf treatments on HCA-7 were characterized by lower Fe/S ratios compared to the corresponding Fe(II) sulfate treatment. Especially in the case of treatments with organic Fe(III) compounds, the Fe/S ratios were dramatically lower for HCA-7 cells (Fig. 2). However, this is understandable solely for the Tf treatments due to the lower TfR1 expression of HCA-7 cells and surprising for the Fe(III) citrate ones.

Study of Fe overload

Characterization of XANES of Fe overloaded cancer cells

The three Fe(III) standards investigated proved to have different XANES (Fig. 3a). Interestingly, the XANES of aqueous Fe(III) sulfate had a sharp decrease of the white line (first maximum of the XANES) with practically no shoulder in the near edge region of the spectra between 7135 and 7140 eV compared to those of deliquescent Fe(III) sulfate and Fe(III) sulfate in DMSO (Fig. 3a). The reason behind this phenomenon is the fact that the dried aqueous Fe(III) sulfate can be characterized with the formula $[Fe(H_2O)_6]_2(SO_4)_3$ [32], where the chemical structure

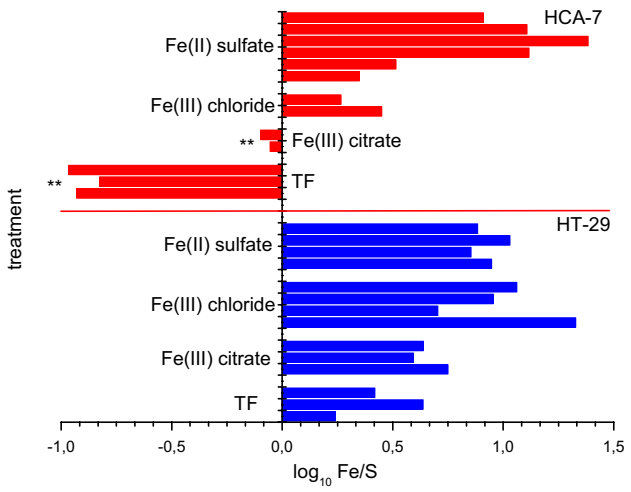

Fig. 2 Iron and sulfur fluorescent signal intensity ratios for HCA-7 and HT-29 human colon adenocarcinoma cells treated with 50 µM Fe(II) sulfate, Fe(III) chloride, Fe(III) citrate and transferrin each on a logarithmic scale with base 10; **, HT-29 versus HCA-7, $p < 0.01$

of the complex ion corresponds to a regular octahedral geometry with an O_h symmetry.

In the present study, the XANES of fast-proliferating HT-29 and slow-proliferating HCA-7 colorectal cells with either Tf or non-Tf type of Fe uptake were recorded. All spectra revealed that Fe was present in the samples in trivalent form. Previously, we reported on the Fe XANES of several Fe standards, among them ferritin. [22]. Moreover, the Fe XANES of cancer cells not subjected to additional Fe treatment [22], resembled those recorded for ferritin standard, since most of cellular Fe is bound to this protein [22].

Independently of the treatment time (4 vs. 24 h), similar XANES were obtained for HT-29 cells with a characteristic shape (Fig. 3b), showing the same shoulder. The shape of shoulder was not affected by the treatment time. Moreover, this characteristic shoulder is in good agreement with the report of Bacquart et al. [33]. However, in the aforementioned report, the focus was on the instrumental analytical aspects of speciation of several elements including Fe at subcellular level in real samples. According to Westre et al., this distorted high spin octahedral geometry can be explained [34] with this spectral phenomenon. This distorted octahedral complex structure suggests the existence of one or two ligands connected loosely to the Fe core allowing for a fast ligand exchange rate necessary for the bioavailability of Fe.

By comparing the Fe XANES resulted upon overloading of HT-29 with Fe(II) sulfate with those of several Fe standards, the spectra of cells resembled mostly the XANES of deliquescent Fe(III) sulfate (Fig. 3b). Moreover, there was less similarity with those of ferritin (Fig. 3b), while the XANES of cells treated with Tf did not show this characteristic shoulder resulting in a ferritin-like spectrum (Fig. 3c). Further, this shoulder was more characteristic for inorganic Fe treatments compared to the Fe transferrin treatment, while it was not so pronounced for Fe(III) citrate treatment (Fig. 3d).

Due to the low Fe content, spectra of HCA-7 treated with either Fe(III) citrate or Tf were difficult to be evaluated. For all HCA-7 samples treated with Fe(II) sulfate, the XANES showed the characteristic shoulder (Fig. 3e, f). The XANES of HCA-7 cells treated with inorganic Fe salts was slightly dependent on the Fe/S ratios. For $\log_{10}$ Fe/S values less than 0.5, the spectra showed a clear shoulder like for deliquescent Fe(III) sulfate (Fig. 3e), whereas XANES of HCA-7 cells, for which the $\log_{10}$ Fe/S value was higher than 0.5, was practically identical to those of Fe(III) sulfate in DMSO (Fig. 3f).

Least squares linear combination (LSLC) fitting of XANES of HT-29 cells

By looking at the XANES spectra, two extremes could be observed, namely, spectra of deliquescent Fe(III) sulfate

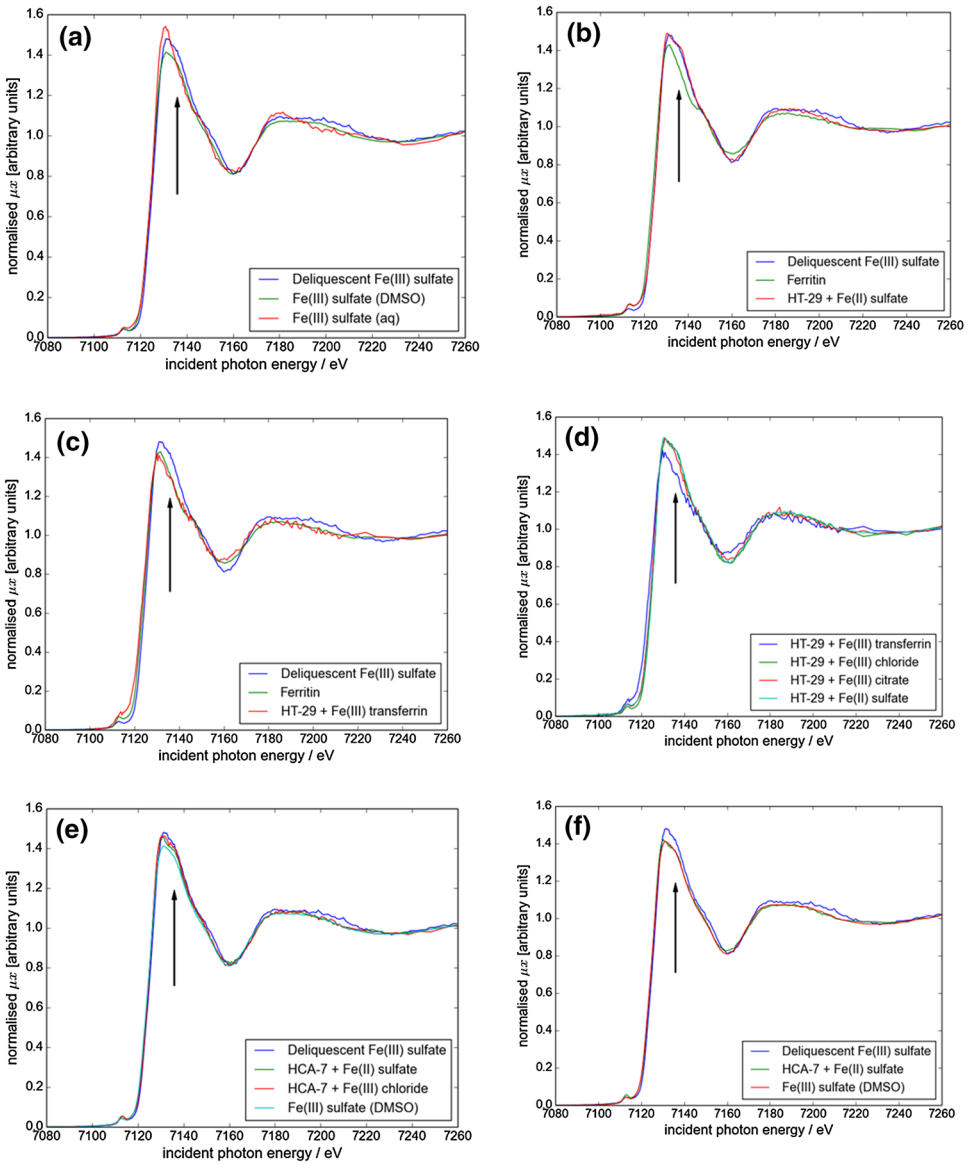

Fig. 3 Comparison of XANES of **a** deliquescent Fe(III) sulfate, Fe(III) sulfate in DMSO and aqueous Fe(III) sulfate standards; **b** deliquescent Fe(III) sulfate, ferritin and a representative HT-29 sample treated with Fe(II) sulfate; **c** deliquescent Fe(III) sulfate, ferritin and a representative transferrin treated HT-29 sample; **d** representative samples of HT-29 cells treated with transferrin, Fe(III) chloride, Fe(III) citrate and Fe(II) sulfate; **e** deliquescent Fe(III) sulfate, representative HCA-7 samples treated with Fe(II) sulfate and Fe(III) chloride with $\log_{10}$ Fe/S ratios less than 0.5 and Fe(III) sulfate in DMSO standard; **f** deliquescent Fe(III) sulfate, a representative sample of HCA-7 cells overloaded with Fe(II) sulfate with $\log_{10}$ Fe/S ratios higher than 0.5 and Fe(III) sulfate in DMSO standard

and of ferritin for characterization of labile Fe pool and intracellular protein of Fe storage, respectively. Thus, it was investigated whether the XANES of Fe overloaded cells containing different Fe compounds could be described as a linear combination of these two extreme components and, thus, an estimation of the combination coefficients was attempted. The results showed that all Fe XANES of HT-29 samples could be clearly described as a linear combination of deliquescent Fe(III) sulfate and ferritin, independently of the chemical form of Fe(III) compounds used for cell treatments (Table 1). The XANES of cells resulting from non-Tf Fe uptake can be modeled using a higher percentage of deliquescent Fe(III) sulfate indicating similarity in the distorted octahedral geometry of this standard and the supposed storing protein system of the studied cell. The LSC fitting is suitable if the spectra obtained from the same type of treatment can be treated as one spectrum. This was possible only in the case of HT-29 cells, where XANES spectra are similar for each Fe treatment.

Table 1 Linear combination (LC) fittings for HT-29 cancer cells treated with different Fe compounds

Fe treatment	LC fitting	R-factor	Chi square
Fe(II) sulfate	100 % Fe(III) sulfate; 0 % ferritin		
Fe(III) chloride	77 % Fe(III) sulfate; 23 % ferritin	0.000267	0.02945
Fe(III) citrate	59 % Fe(III) sulfate; 41 % ferritin	0.000512	0.05554
Transferrin	8 % Fe(III) sulfate; 91 % ferritin	0.001340	0.14221

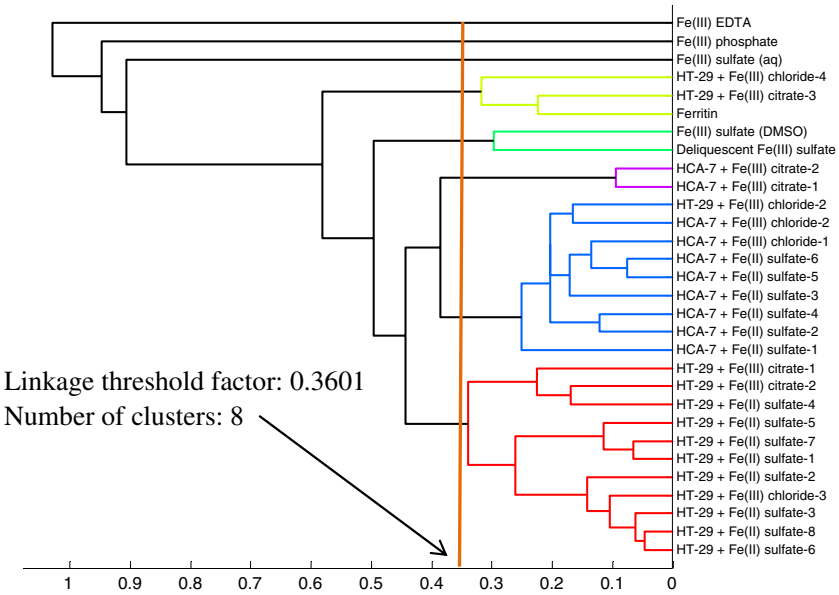

Fig. 4 Dendrogram of agglomerative hierarchical cluster tree for Fe XANES of different standards and Fe overloaded HT-29 and HCA-7 human colon adenocarcinoma cells

PCA–hierarchical clustering analysis of XANES

By performing hierarchical cluster analysis for all of the XANES recorded [Fe(II/III) standards selected from [22] and HT-29 and HCA-7 cells treated with Fe(II/III) standards], samples could be classified into eight clusters (Fig. 4). It should be emphasized that Fe XANES of samples treated with Tf was omitted from the PCA–hierarchical clustering, because these individual spectra were too noisy for statistical data evaluation. The XANES of three of the investigated Fe(III) standards—Fe(III) EDTA, Fe(III) phosphate and aqueous Fe(III) sulfate—differed considerably from each other and all other recorded XANES and thus, formed three individual clusters (linkage distance >80 % of the maximum linkage distance, see Fig. 4). The XANES of HCA-7 samples treated with either Fe(III) chloride or Fe(II) sulfate was pooled into one cluster, whereas those treated with Fe(III) citrate constituted a separate cluster. Independently of the Fe treatment type for HT-29 cells, all of their XANES except one could be grouped into one cluster clearly differentiating them from the XANES of HCA-7 samples (linkage distance >40 % of the maximum distance). In the case of HCA-7 samples two subsets were found, one containing only spectra of inorganic Fe treatments and a second one corresponding to the Fe(III) citrate treatment (Fig. 4). A separate cluster was obtained for the XANES of deliquescent Fe(III) sulfate and that dissolved in DMSO. However, inspection of the individual XANES showed that these two standards resemble the XANES of the samples having the shoulder. Besides these clear groups, three outliers were identified: the spectrum of one of the HT-29 samples treated with Fe(III) chloride could not be distinguished from those of the HCA-7 samples, and the XANES of two other HT-29 samples (HT-29 cells treated with Fe(III) chloride and Fe(III) citrate) was found to be similar to the one recorded for ferritin. Thus, the latter two formed a separate group together with the ferritin reference. The most probable reason for these two outliers is a damping and/or a distortion of the XANES features due to self-absorption effects caused by either an outstanding Fe/S ratio (approx. 1.4) or a high cell number, respectively. The clustering result further supports the choice of ferritin and deliquescent Fe(III) sulfate as references in the LSLC fitting being the standards with most similar XANES to those of the cell samples.

Thus, among the 24 cell sample spectra recorded, only one cell sample was misclassified, namely one HT-29 cell sample treated with Fe(III) chloride (Fig. 4). However, hierarchical cluster analysis based on the spectra features of Fe K-edge XANES revealed that the chemical structure of the Fe pool—presumably a protein system—is different for the studied two human carcinoma cells. This could be revealed by clustering of spectra of different cell lines treated with Fe.

XRF imaging of Fe overloaded HT-29 cells

Micro-XRF imaging of Fe loaded HT-29 cells was achieved at a resolution of 0.5 μm × 1 μm. For the acquisition of the XRF image of the Fe loaded HT-29 cells, supplementation of the cell culture with 50 μM of Fe(II) sulfate is ideal due to the high accumulation rate of this Fe(II) compound in this type of cancer cell line [19]. Cell boundaries could be visualized by mapping physiologically relevant elements such as Cl and K, whereas cell nuclei could be identified using the Zn signal (Fig. 5). According to our results and

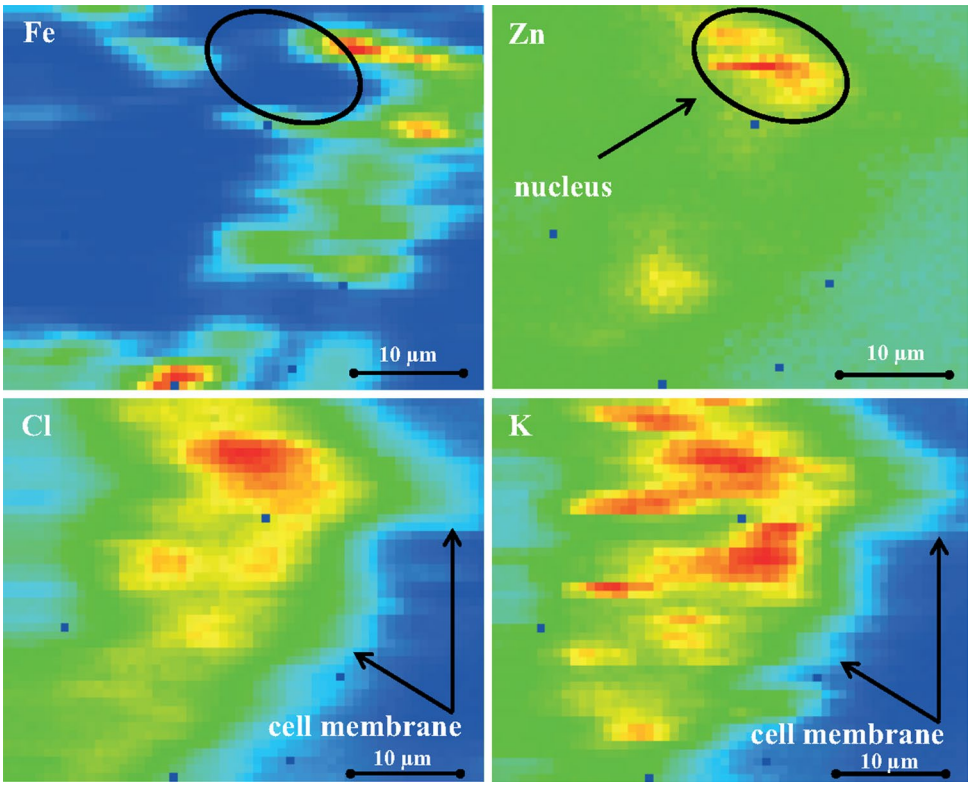

Fig. 5 False-color XRF image (45 µm × 30 µm) showing iron, zinc, chlorine and potassium distribution in HT-29 cells supplemented with 50 µM Fe(II) sulfate. The relative intensities increase in the order *blue*, *green*, *yellow*, *orange* and *red*

not surprisingly, Fe could be detected exclusively in cytosol and not in the nuclei characterized by a high Zn content. However, at other methods, Fe and nuclei are visualized by fluorescence chelator and DNA dyes (i.e., Hoechst stain), respectively [18]. Moreover, the cellular distribution of Fe proved to be diffuse and Fe accumulation could not be observed. However, there were some indications about Fe compartmentalization within the cells (Fig. 5).

Conclusion

By investigating one fast- and one slow-proliferating adenocarcinoma cancer cell line—HT-29 and HCA-7—with high and low TfR1 expression, respectively, the extent of the inorganic Fe uptake by the two cells was found to be similar. The same decreasing order in Fe/S ratios according to the different treatments was observed for both cells: Fe(II) sulfate > Fe(III) chloride > Fe(III) citrate > Tf but there was a considerable difference in the Fe/S ratios for the treatments with organic Fe. For HCA-7 cells characterized by lower TfR1 expression, the dramatically lower Fe/S ratios were understandable for Tf treatments but unexpected for Fe(III) citrate ones.

When overloaded with inorganic Fe(II/III), a specific shoulder in the XANES for both cells in the near edge region of spectra independently of the treatment time (4 vs. 24 h) was observed. These XANES spectra resembled mainly to those of deliquescent Fe(III) in the aqueous form. However, regardless of the Fe treatment, the two cells could be differentiated unequivocally and without any a priori knowledge by their XANES signature using hierarchical cluster analysis. This can be related to different Fe storage systems in the case of Fe overload. The results for Tf loaded cells suggest ferritin-like spectrum. The XANES of HT-29 cells could be described as the linear combination of the XANES of deliquescent Fe(III) sulfate and ferritin indicating that Fe can only exist in the cells either in the labile pool or ferritin storage but in different percentage.

The differences observed represent a step closer toward understanding Fe overload conditions of cancer cells.

Acknowledgments The technical as well as financial supports from DESY and Diamond Light Source contract No I-20110800 EC and 10230, respectively, are hereby acknowledged. The authors express their gratitude to Ian Pape and Kawal J. S. Sawhney for their efforts made in preparing the X-ray imaging experiments. The research leading to these results has also received funding from the European Community's Seventh Framework Programme (FP7/2007–2013) under Grant agreement No 226716.

References

1. Walker BL, Tiong JW, Jefferies WA (2001) Int Rev Cytol 211:241–278
2. Hentze MW, Muckenthaler MU, Andrews NC (2004) Cell 117:285–297

3. Dhungana S, Taboy CH, Zak O, Larvie M, Crumbliss AL, Aisen P (2004) Biochemistry 43:205–209
4. Ohgami RS, Campagna DR, Greer EL, Antiochos B, McDonald A, Chen J, Sharp JJ, Fujiwara Y, Barker JE, Fleming MD (2005) Nat Genet 37:1264–1269
5. Kwok JC, Richardson DR (2002) Crit Rev Oncol Hematol 42:65–78
6. Dominici S, Pieri L, Comporti M, Pompella A (2003) Cancer Cell Int 3:7–14
7. Adams PC, Barton JC (2007) Lancet 370:1855–1860
8. Kohgo Y, Ikuta K, Ohtake T, Torimoto Y, Kato J (2008) Int J Hematol 88:7–15
9. Kakhlon O, Cabantchik ZI (2002) Free Radic Biol Med 33:1037–1046
10. Liuzzi JP, Aydemir F, Nam H, Knutson MD, Cousins RJ (2006) Proc Natl Acad Sci USA 103:13612–13617
11. Gunshin H, Mackenzie B, Berger UV, Gunshin Y, Romero MF, Boron WF, Nussberger S, Golan JL, Hediger MA (1997) Nature 388:482–488
12. Mackenzie B, Ujwal ML, Chang MH, Romero MF, Hediger MA (2006) Pflügers Arch 451:544–558
13. Breuer W, Shvartsmann M, Cabantchik I (2008) Int J Biochem Cell Biol 40:350–354
14. Sturrock A, Alexander J, Lamb J, Craven CM, Kaplan J (1990) J Biol Chem 265:3139–3145
15. Epsztejn S, Kakhlon O, Glickstein H, Breuer W, Cabantchik I (1997) Anal Biochem 248:31–40
16. Petrat F, de Groot H, Sustmann R, Rauen U (2002) Biol Chem 383:489–502
17. Prus E, Fibach E (2008) Br J Haematol 142:301–307
18. Au-Yeung HY, Chan J, Chantarojsiri T, Chang CJ (2013) J Am Chem Soc 135:15165–15173
19. Polgári Z, Ajtony Z, Kregsamer P, Streli C, Mihucz VG, Réti A, Barna B, Kralovánszky J, Szoboszlai N, Záray G (2011) Talanta 85:1959–1965
20. Szoboszlai N, Polgári Z, Mihucz VG, Záray G (2009) Anal Chim Acta 633:1–18
21. Meirer F, Singh A, Pianetta P, Pepponi G, Meirer F, Streli C, Homma T (2010) TrAC 29:479–496
22. Polgári Z, Meirer F, Sasamori S, Ingerle D, Pepponi G, Streli C, Rickers K, Réti A, Budai B, Szoboszlai N, Záray G (2011) Spectrochim Acta B 66:274–279
23. Meirer F, Pepponi G, Streli C, Wobrauschek P, Mihucz VG, Záray G, Czech V, Broekaert JAC, Fittschen UEA, Falkenberg G (2007) X-Ray Spectrom 36:408–412
24. Meirer F, Pepponi G, Streli C, Wobrauschek P, Kregsamer P, Zoeger N, Falkenberg G (2008) Spectrochim Acta B 63:1496–1502
25. Ravel B, Newville M (2005) J Synchrotron Radiat 12:537–541
26. Sawhney KJS, Dolbnya IP, Tiwari MK, Alianelli L, Scott SM, Preece GM, Pedersen UK, Walton RD (2010) AIP Conf Proc 1234:387
27. Okazaki F, Matsunaga N, Okazaki H, Utoguchi N, Suzuki R, Maruyama K, Koyanagi S, Ohdo S (2010) Cancer Res 70:6238–6246
28. Neckers LM, Trepel JB (1986) Cancer Invest 4:461–470
29. Szoboszlai N, Réti A, Budai B, Szabó Z, Kralovánszky J, Záray G (2008) Spectrochim Acta B 63:1480–1484
30. Olivieri NF (1999) N Engl J Med 341:99–109
31. Galanello R, Origa R (2010) Orphanet J Rare Dis 5:11–26
32. Asakura K, Nomura M, Kuroda H (1985) Bull Chem Soc Jpn 58:1543–1550
33. Bacquart T, Devès G, Carmona A, Tucoulou R, Bohic S, Ortega R (2007) Anal Chem 79:7353–7359
34. Westre TE, Kennepohl P, DeWitt JG, Hedman B, Hodgson KO, Solomon EI (1997) J Am Chem Soc 119:6297–6314